AIAA JOURNAL
Vol. 46, No. 11, November 2008

Investigation of the Magnetic Field in a Pulsed Plasma Thruster

Anuscheh Nawaz,* Matthias Lau,† Georg Herdrich,‡ and Monika Auweter-Kurtz§
University of Stuttgart, 70569 Stuttgart, Germany

DOI: 10.2514/1.37161

The magnetic field between the electrodes of an 80 J ablative pulsed plasma thruster was both measured and determined analytically. This was done to better understand the acceleration process and assess the accuracy of the analytical method. The measurements at different positions in both breech-fed and side-fed propellant configurations were performed using a shielded induction probe of 1 mm in diameter. To calibrate the probe, a Helmholtz coil was built. The magnetic field was calculated using the law of Biot–Savart and assuming a current sheet thickness of 3 mm. The measured magnetic field showed an overall peak at 0.7 T. It was possible to confirm the induced current loop formed between the electrodes at the time when the overall current passes through zero. The comparison between the magnetic field model and the measurements at the propellant surface of a breech-fed thruster showed reasonably good accordance.

Nomenclature

A	=	area, m^2
B	=	magnetic field, T
C	=	capacitance, F
d	=	width of the electrodes, m
E	=	electric field, V/m
E_0	=	bank energy, J
h	=	electrode gap, m
I	=	current, A
j	=	current density, A/m^2
L	=	inductance, Tm^2/A
N	=	number of turns in coil
R_H	=	radius of Helmholtz coil, m
$\mathbf{r}$	=	position vector, m
U	=	voltage, V
U_V	=	vector potential, Vs/m
u_i	=	induced voltage, V
α	=	integration angle, rad
ϵ	=	sensitivity for probe calibration, m^2
μ	=	magnetic permeability, H/m
ρ	=	perpendicular distance from point to wire, m
Φ	=	magnetic flux, Tm^2
ω	=	angular frequency, 1/s

I. Introduction

NONSTATIONARY magnetoplasmadynamic thrusters, also known as pulsed plasma thrusters (PPTs), are used on satellites for stationkeeping and orbit control. Because of their robust design and flexibility regarding their power consumption, these thrusters are ideally suited for small satellites. They can also be used as the main propulsion system on small satellites, promoting high payloads [1]. Using electromagnetic forces, these electric thrusters accelerate plasma formed between their electrodes and expel it at mean exhaust velocities between 3 and 50 km/s, depending on the thruster's energy level [2]. PPTs can be classified through their solid or gaseous propellant, their propellant feed configuration, and the geometry of the electrodes. When using solid propellant, they are called ablative pulsed plasma thrusters (APPT). A parallel electrode APPT will be discussed in the following.

Figures 1a and 1b show a sketch and a picture of the thruster, respectively. During one discharge pulse, the energy stored in capacitors is released. When the igniter is fired, the pulse is initiated by short-circuiting the capacitors across the polytetrafluoroethylene (PTFE) propellant bar. Independent of the bar geometry, the initial discharge takes place across the surface, ablating and partially ionizing the PTFE. The plasma forming during this process is the only nonfixed part of the discharge circuit. The current through the plasma interacts with the circuit's own magnetic field, causing an electromagnetic force on the plasma sheet along the electrodes. As a result of this Lorentz force, the current sheet is expelled from the thrusters exhaust. Because the particle velocity and the magnetic field as well as the circuit boundaries are functions of time and space, the measurement and calculation is complex. However, knowledge of the spacial and temporal magnetic field distribution plays a vital role in modeling the Lorentz force acceleration and deriving the circuit inductance. Both of these functions are required for understanding and modeling the thruster's physics and ultimately lead to optimizing the thruster. This work presents an approach to understanding the magnetic field behavior and development, both from the experimental and the modeling side.

The magnetic field was measured by using an induction coil. Even though a Hall-effect sensor would pose a viable option, the induction coil technique for determining the magnetic field has been successfully used in the past by several other researchers [3–5]. Palumbo and Begun [6] measured the magnetic field between the electrodes of an 81.9 J parallel plate accelerator. In his latest research, Koizumi et al. [5] used the magnetic field to aid analysis from optical measurement techniques. The magnetic field was measured with a very high spatial resolution, albeit outside the acceleration channel. Research done herein measures the magnetic field at different positions directly inside the channel. To optimize the accuracy of the measurement, the sensor developed was calibrated carefully and shielded from electromagnetic noise. Measurements were conducted for a breech-fed and a side-fed thruster configuration. It was possible to compare the breech-fed data within the acceleration channel to a model, using the Biot–Savart law.

II. Analytical Method

For solid propellant thrusters, the main mechanisms of the discharge [7] are described by the *slug model*. Within this model, the complete ablated mass bit moves along the electrodes as a thin

Received 18 February 2008; revision received 7 July 2008; accepted for publication 7 July 2008.

*Doctoral Candidate, Space Transportation, Institute of Space Systems; nawaz.anuscheh@googlemail.com

†Graduate Research Student, Space Transportation, Institute of Space Systems; lau@irs.uni-stuttgart.de.

‡Section Head, Space Transportation, Institute of Space Systems; herdrich@irs.uni-stuttgart.de. Member AIAA.

§President, University of Hamburg; praesidentin@hvn.uni-hamburg.de. Fellow AIAA.

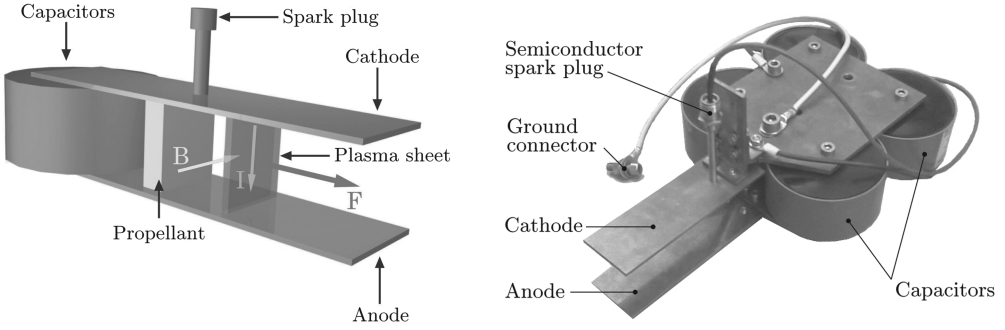

a) Working principle of a PPT **b) SIMP-LEX thruster used for magnetic investigation**

Fig. 1 SIMP-LEX thruster and working principle.

plasma sheet, accelerated by the Lorentz force. In reality, the plasma is only partially ionized and the sheet is not thin, nor is it perpendicular to the electrodes at all times. However, the model captures the basic physics of the thruster and allows one to establish influence parameters.

The magnetic field **B** of an APPT plays an important role, both when modeling the Lorentz acceleration force and when deriving the change in inductance $\Delta L = \int \mathbf{B}\,\mathrm{d}\mathbf{A}/I$ as a function of time. Here, **A** stands for the area enclosed by the circuit loop, carrying the current I, and is constantly changing as the plasma moves along. A magnetic field is caused by the movement of ionized particles, that is, current. To calculate the magnetic field at any given point of the thruster, the contributions of all parts of the circuit have to be added at the point of interest. The derivation of the Biot–Savart [8] equation, relating the spatially varying magnetic field to the current density, is based on the Maxwell equations:

$$\nabla \times \mathbf{B} = \mu \mathbf{j} \tag{1}$$

$$\nabla \cdot \mathbf{B} = 0 \tag{2}$$

Here μ represents the magnetic permeability. This approach neglects the partial derivative of the electric field with respect to time in Eq. (1) due to the steady state nature of the approach. The Biot–Savart law is stated in Eq. (3):

$$\mathbf{B}(\mathbf{r}) = \frac{\mu_0}{4\pi} \int \frac{\mathbf{I}(\mathbf{r}') \times (\mathbf{r} - \mathbf{r}')}{|\mathbf{r} - \mathbf{r}'|^3}\,\mathrm{d}s \tag{3}$$

The magnetic field contribution of ds in point $P(\mathbf{r})$ is perpendicular to both the current and the vector pointing from the wire element ds to the point **P**. Note that Eq. (3) is derived for steady fields, because the electric displacement was neglected in Ampere's law, Eq. (1). However, at the thruster frequency of 100 kHz the fraction of the displacement current is on the order of 10^{-14} of the total current, according to the theory of electromagnetic waves in conducting materials, neglecting polarization [8]. This corresponds to a value of -275 dB, as seen in Fig. 2. This figure shows the bode diagram of the ratio between the displacement current and the total current. The plasma frequency for copper electrodes is 1.6×10^{16}, assuming values of 8.5×10^{28} $1/\mathrm{m}^3$ and 2.4×10^{-14} s for the electron density and average time between collisions, respectively.

The discharge is modeled by using an extended slug model, where the magnetic field is calculated according to the law of Biot–Savart in Eq. (3) for calculating the magnetic field contributions from the electrodes. The relevant assumptions made in the model are as follows: The electrodes are of zero thickness and are modeled by current wires only. The capacitors are represented by a current sheet, similar to the plasma sheet: the complete circuit is modeled. The plasma sheet is perpendicular to the electrodes at all times. The thickness of the plasma sheet is constant at 3 mm. The mass of the plasma sheet is constant during the acceleration process. The mass bit is divided into three plasma sheets proportional to the current integral of the half-period. The electrodes are 87 mm long.

The modeling of the magnetic field between the electrodes is done in three steps. The first step is the determination of the change in inductance over the plasma position from the given electrode geometry of the thruster, using the law of Biot–Savart. A discrete three-dimensional grid divides the volume described by the width, the length between the plasma sheet and the PTFE bar, and the distance between the electrodes in 100 steps along each axis direction. The plasma-sheet step distance in x direction is the 100th part of the electrode length. One-hundred parallel current wires represent one electrode. Their length is determined by the electrodes, and each carries the respective fraction of the overall current. The contribution of the plasma sheet to the magnetic field between the electrodes is calculated at the same grid points. The plasma sheet assumes current wires of infinite length in a two-dimensional configuration and a constant current density inside the plasma. The calculated discrete $\Delta L(x)$ is approximated by a fourth-order polynomial for implementation in the slug model. For the second step, the differential equations of the slug model are solved one first time to calculate the discharge current. The measured massbit of the considered thruster configuration is then divided into three fractions for the three plasma sheets of the staged calculation. The massbit of the first sheet equals the ratio between the area determined by the integral across the first half-cycle and the overall area of the current curve. The second massbit refers to the second half-cycle, whereas the remaining mass is all assigned to the third and final sheet. Assuming these three massbits, three calculation runs yield the temporal plasma position and the discharge current for each plasma sheet. The third step uses the same routines and grids described for the first step. The probe's location between the electrodes is approximated by a grid point. The magnetic field per current is calculated at this point for all plasma positions. As long as the plasma sheet has not yet passed the probe location, only the magnetic field of the sheet is considered. The obtained magnetic field over time at the probe is multiplied with the current from the slug model. In

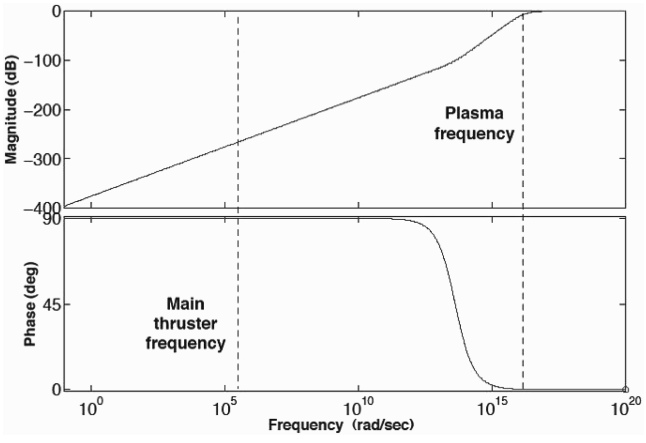

Fig. 2 Bode plot of the ratio between displacement current and total current.

combination with the temporal position of the three plasma sheets, this leads to the magnetic field signals presented in this work.

To evaluate the influence of the current sheet on the circuit's inductance, calculations with sheets of 0, 3, and 15 mm thickness were run. Figure 3a shows the calculated change in inductance over x along the electrodes. A distinct increase in the inductance change appears with the presence of a current sheet.

The ratio between the change in inductance with and without a current sheet is seen in Fig. 3b. Both ratios show a peak, indicating that the maximum aberrations occur when the current sheet is close to the propellant surface. Increasing the thickness of the sheet causes the peak to decrease and delay, because the sheet's current density decreases accordingly. With increasing distance to the propellant, the contribution of the sheet's magnetic field to the remaining circuit's magnetic field decreases, causing the two ratio graphs to close in and decline over x.

III. Induction Probe Calibration

The underlying physics of the induction coil used for measuring the thruster's magnetic field is based on the Faraday equation for constant areas A:

$$u_i = \oint_{\partial A} \mathbf{E}\,\mathrm{d}\mathbf{s} = -\frac{\mathrm{d}}{\mathrm{d}t}\int_A \mathbf{B}\,\mathrm{d}\mathbf{A} \tag{4}$$

The change in magnetic field **B** causes an electric field **E** along the closed integration curve **s**. The induced voltage u_i can be recorded. The induction behavior of the coil strongly depends on the frequency of the changing magnetic field. Recording of the capacitor voltage during a discharge reveals the frequency spectrum to be expected from a transient magnetic field measurement. The induction coil's response to those frequencies must not distort the measured signal, hence a calibration of the probe has to be performed to check the coil's output. The coil's change of the magnitude and phase of a signal must be known as a function of the frequency. The lower frequency limit of a coil is given by its own ohmic resistance. In this case, the limit is reached if voltages induced by low frequencies are in the range of the coil's falling ohmic voltage. The upper frequency limit of the coil is due to increasing capacitive effects and the coil's natural frequency. For the magnetic field probe in Fig. 4, a small induction coil was built. It is made of one layer of 15 turns using 0.2 mm insulated copper wire around a hollow plastic core. The number of turns provides good sensitivity for changes in the magnetic field. The coil has a diameter of 1 mm and a total length of 3.5 mm. Layers of aluminum foil shield the coil and its wires from electric fields. In addition to feeding the wire back through the probe's core, the wires leading up to the probe are twisted. This avoids unwanted magnetic coupling. To insulate the probe from the plasma, the wrapped coil is put inside a glass tube with an outer diameter of 6 mm. The probe's design allows one to measure between the thruster's electrodes, whereas the coil's small size provides a high local resolution.

The voltage spectrum mirrors the frequencies the magnetic field sensor is exposed to, because the magnetic field is related to the thruster's discharge current and is thus connected to the capacitor's discharge voltage. The spectrum shows a peak at 100 kHz and fading magnitudes above 300 kHz, thus the calibration limit for the induction coil was set to 300 kHz. It is critical for the design of the induction probe to avoid any areas formed by the wire other than the one described by the coil turns. In particular, connecting the wires at both ends of the coil creates an area perpendicular to the coil's turns. This area acts like a single turn induction coil responding to components of the magnetic field that are perpendicular to the coil's axis. The effect of unwanted coupling was avoided by leading the coil's enameled copper wire through the coil's hollow core.

To calibrate the probe, a uniform magnetic field with adjustable alternating frequency and of known magnitude $B(t)$ is required. A Helmholtz coil approach was chosen for this purpose. The Helmholtz calibration coil used consists of a set of two coils with 30 windings each and a 2 cm radius, wound with 0.2 mm enameled copper wire. The distance between the coils' centers equals their radius, according to the Helmholtz condition. The Helmholtz coil's natural frequency of 10 MHz was high enough to have no effect on the calibration.

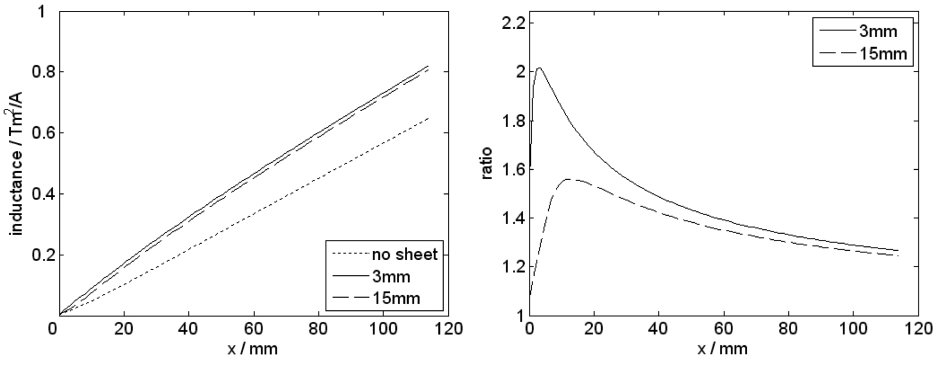

a) Calculated circuit inductance change **b) Effect of a finite plasma sheet on circuit inductance**

Fig. 3 Influence of the current sheet and its thickness on circuit inductance, 2000 V bank voltage.

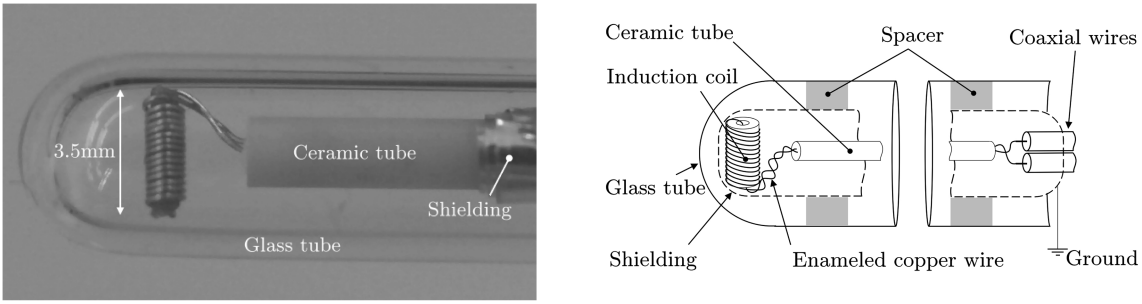

a) Head of induction probe **b) Schematic view of the induction probe**

Fig. 4 Induction magnetic field probe.

Depending on the frequency, B varied between 1 and 50 mT inside the Helmholtz coil.

The following section describes the calibration of the induction coil by means of the Helmholtz coil setup. Any alternating magnetic field can be described by

$$B(t) = B_0 e^{j\omega t} \tag{5}$$

with the amplitude B_0, time t, and angular frequency ω. From Faraday's law, the induced voltage u_i of a coil of N turns and a constant area A is calculated according to Eq. (4).

Applying the derivative of Eq. (5) to Eq. (4) yields the induced voltage in the coil:

$$u_i = -NAj\omega B_0 e^{j\omega t} \tag{6}$$

The amplitude $\hat{u}_i = NA\omega B_0$ can be considered to be the theoretical reference for the measured voltage amplitude $\hat{u}_{\text{exp}}$ of the probe at a given frequency. To obtain B_0, the analytical treatment for Helmholtz coils is applied [9]:

$$B(z) = \frac{8}{\sqrt{125}}\mu_0 \frac{NI_0}{R_H}\left[1 - \frac{144}{125}\left(\frac{z}{R_H}\right)^4\right] \tag{7}$$

Here, R_H is the radius of the Helmholtz coil. The variable I_0 is the amplitude of the induced current, which can be determined by measurement. The distance from the center point between the two annular coils on their joint axis is described by z. For a probe positioned at $z = 0$, Eq. (7) reduces to

$$B_0 = \frac{8}{\sqrt{125}}\mu_0 \frac{NI_0}{R_H} \tag{8}$$

Because the length of the probe's coil cannot be neglected and the magnetic field changes over z, a qualitative error can be determined. However, this error can be neglected [10] as it is less than 1% for a ratio $z/R_H \geq 0.3$. To better visualize the comparison between the theoretically induced voltage u_i and the measured induced voltage u_{exp}, the sensitivity ϵ is introduced:

$$\epsilon_{\text{exp}} = \frac{\hat{u}_{\text{exp}}}{\hat{u}_i/nA} = \frac{\hat{u}_{\text{exp}}}{\omega B_0} \tag{9}$$

For an ideal response of the probe to the magnetic field, the magnitudes of u_{exp} and u_i will be equal and ϵ will become $\epsilon_{\text{th}} = nA$. The experimental setup to obtain I_0 and $\hat{u}_{\text{exp}}$ is shown in Fig. 5a.

The Helmholtz coil was connected to a frequency generator, acting as a power supply. A passive Tektronix P6021 current monitor passed the current signal I_0 to a two-channel oscilloscope. The second channel recorded the induced voltage signal $\hat{u}_{\text{exp}}$ provided by the induction probe. To gain signal strength, the induced voltage was multiplied tenfold by a differential amplifier. The results of the calibration are given in Fig. 5b. The curves show good correlation over the entire calibration range, which means there is a high probe response accuracy. The error bars of up to −21% mainly reflect aberrations due to a possibly smaller Helmholtz radius, along with errors from reading off the analog frequency generator.

IV. Experimental Setup

Magnetic field measurements were conducted in a cylindric vacuum chamber, at base pressures of 2×10^{-4} mbar. A combination of a rotary vane pump and a turbopump maintained a steady pressure level during tests. The chamber and the thruster's cathode were grounded. The chamber is accessible via two flanges to adjust the experimental setup. An outside view of the chamber is given in Fig. 6a.

The thrusters bank energy of <80 J was provided by a power supply with a maximum voltage of 2000 V. The semiconductor spark plug for single-shot discharge initiation was triggered manually and operated at 1000 V. Inside the chamber, the thruster was mounted on an insulating rail to allow for flexible thruster positioning along the electrode axis. The magnetic field probe was attached to a two-axis table, installed in front of the thruster's exhaust. This table could be moved remotely parallel to the thruster's electrode axis. Two

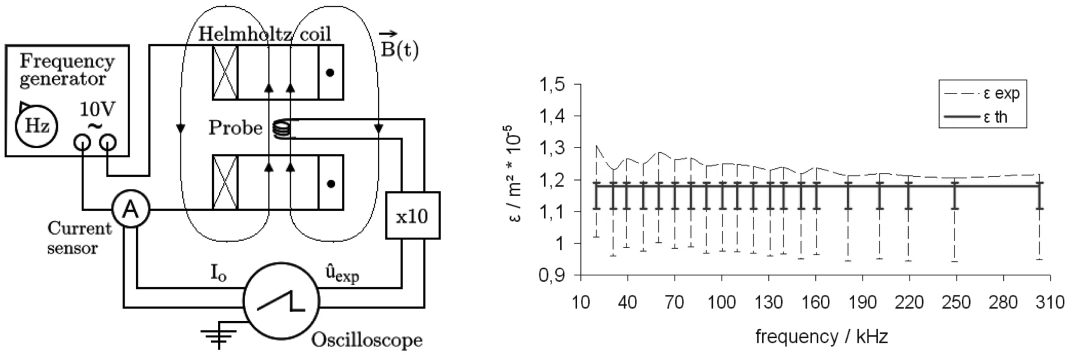

a) Calibration setup b) Calibration curve

Fig. 5 Calibration of the magnetic field probe.

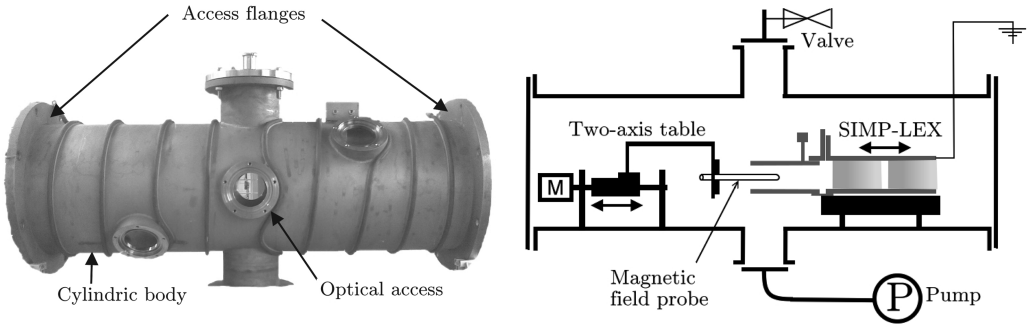

a) Outside view of the chamber b) Schematic view of the test setup

Fig. 6 Test setup inside of the vacuum chamber.

Table 1 Parameters of PPT investigated

d	Width of the electrodes	40 mm
h	Distance between electrodes	36 mm
C	Total capacitance	40 F
E_0	Bank energy	80 J
-	Propellant configuration	side-fed/breech-fed

windows perpendicular to the thruster's axis grant optical access to the vacuum chamber. The setup is shown in Fig. 6b. An engineering model of the PPT under development as the main propulsion system for Baden Wuerttemberg 1 (BW1, the name of the lunar mission) (SIMP-LEX) allows for modification of its geometrical and electrical parameters, such as electrode width, distance between electrodes, and voltage. Systematically choosing the experiment configuration allows for comparison to data recorded from earlier investigations, as well as from literature. The geometric and electric parameters are given in Table 1.

The measurements were conducted charging the capacitors to 1500, 1800, or 2000 V for different test conditions. Two propellant configurations were investigated within this study. The side-fed configuration feeds propellant from both sides perpendicular to the electrode axis at an angle of 53 deg, creating a V shape, as seen in Fig. 7a. The breech-fed configuration in Fig. 7b feeds the PTFE from behind the igniter. This configuration is common for investigations found in literature and was included as a reference configuration.

The magnetic field was measured at five points along the electrode axis, as outlined in Fig. 7b. These measurements were conducted for both propellant feed configurations. To further investigate the side-fed version, three points in the PTFE exit plane and two points on the electrode axis between the propellant bars were added. The magnetic field was assumed to be symmetrical with respect to the x–z plane.

V. Results

In the following section, the influence of capacitor voltage and measurement position on the magnetic field signals for the breech-fed configuration is depicted. The effects detected are then compared with the corresponding data of the side-fed configuration, yielding differences in behavior of plasma acceleration. It is followed by the investigation of the propellant's exit plane. An investigation on the accuracy of modelling the magnetic field is presented last.

Following Eq. (6), with $u_i = LI$, the probe detects the change in magnetic field, caused by the change of both the current and the inductance of the thruster's discharge circuit. Hence, two oppositional effects are important for the interpretation of the measured signal: the relative distance of the probe to the current sheet center and the temporal magnitude of the discharge current. The current sheet thickness plays an important role, as the probe displays the interfering contributions from currents in front of and behind its center. Note that the current sheet differs from the plasma sheet, because the plasma contains nonionized particles.

A. Breech-Fed Configuration

Figure 8a shows the induction signal varying the capacitor voltage at a probe position 5 mm from the propellant's surface. No significant disturbances can be detected on the signal's graph, leading to the conclusion that the electromagnetic shielding of the probe was sufficient. The signal reflects the oscillatory behavior of the thruster's discharge. Integrating the signal leads to the magnetic field distribution, as seen in Fig. 8b. The small negative amplitude at about 1 μs is a result of the gap between the center of the probe and the propellant surface. The current sheet forms at the propellant's surface and induces a signal before the center of the sheet moves past the probe for the remainder of the discharge. Maximum amplitudes increase with initial capacitor voltage. Further, the periodic time is

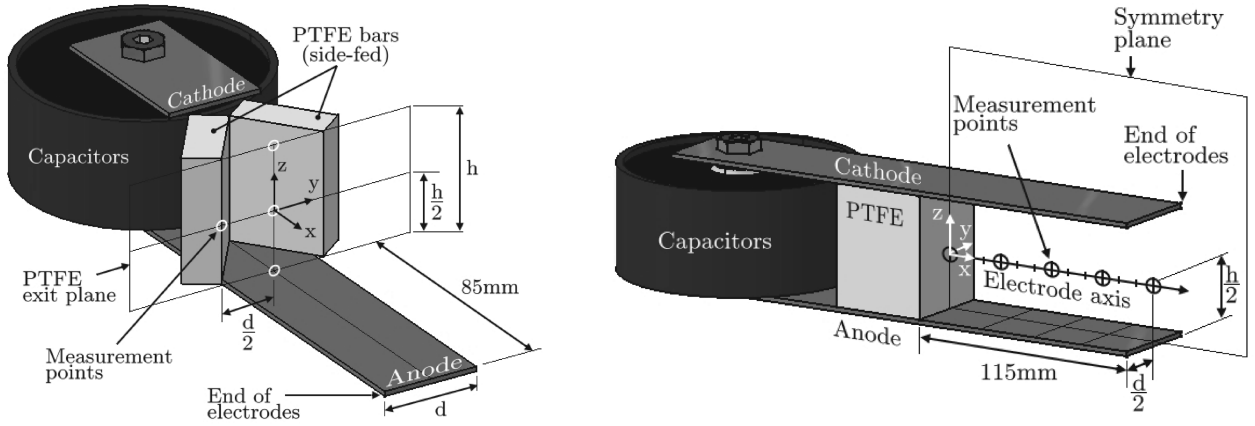

a) Side-fed configuration (cathode displayed shortened) b) Breech-fed configuration (igniter not shown)

Fig. 7 SIMP-LEX: configurations and definitions.

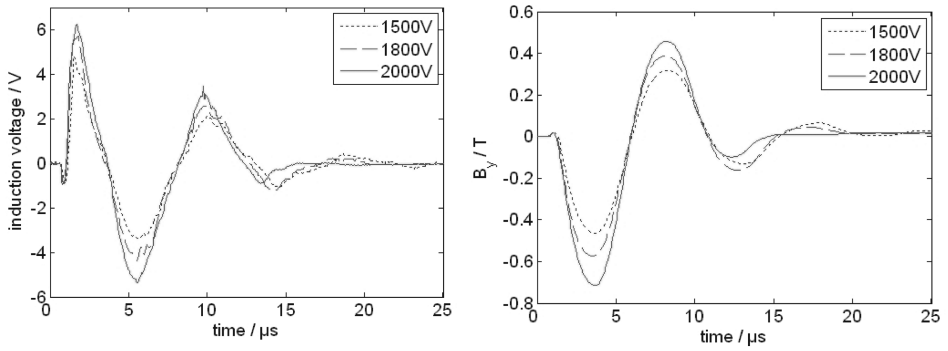

a) Signal from induction probe b) Corresponding magnetic field

Fig. 8 Analysis of induction probe signal for breech-fed thruster at the propellant's exit plane

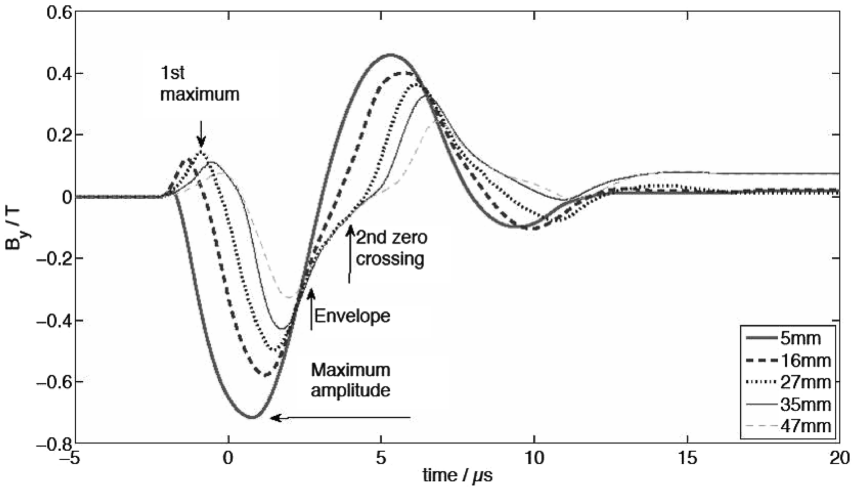

Fig. 9 Signals of induction probe at different positions along the electrode axis, breech-fed, 2000 V.

the same for all three signals. The maximum value for the breech-fed magnetic field is −0.7 T at 2000 V capacitor voltage.

To axially assess the magnetic field, the center of the probe was positioned 5, 16, 27, 35, and 47 mm from the propellant surface, as shown in Fig. 7b. Three half-periods are discernible for all locations in Fig. 9. The four areas highlighted will be discussed later. The magnetic field maximum changes in amplitude and time of occurrence. The magnitude of the first amplitude increases up to a distance of 27 mm, after which it decreases again. This can be explained by recalling that two oppositional effects play a role during the formation of the plasma sheet. A position further away from the propellant surface allows the current to rise higher before crossing the probe. However, if the center of the probe is situated at any point within the current-carrying plasma sheet as the maximum current is reached, the magnetic field registered by the probe decreases due to the averse effect from the current flowing behind the probe.

The magnetic field is zero at the probe, when the effective currents in front of and behind the probe are equal in magnitude, and their magnetic field contributions therefore cancel out. This point can be regarded as the center of the current sheet. As the maximum amplitude of the magnetic field is reached, the position of the probe influences the magnitude: A position further from the propellant surface is associated with a lower magnetic field. This is because, as the probe is positioned further away from the propellant surface, it registers smaller magnetic fields, because current is flowing in front of and behind the probe. Maximum amplitudes are reached later for probe positions further downstream, because the probe is inside the current-carrying sheet at the time of maximum current. Hence, the magnetic field at the probe decreases as the probe position is closer to the center of the current sheet. At the time of maximum current, the probe at 5 mm only sees current on the downstream side and can thus reveal the time when the maximum current is reached.

The second zero crossing does not occur at the same time for all positions. A zero crossing denotes the time when either the discharge current is zero or the magnetic field contributions in front of and behind the probe cancel out. For the 5 mm position, the first is the case. However, for the other positions, a different effect has to be taken into account. As Palumbo and Begun [6] explain in detail, a second current sheet is induced close to the propellant's surface around the time the discharge current passes through zero. This effect

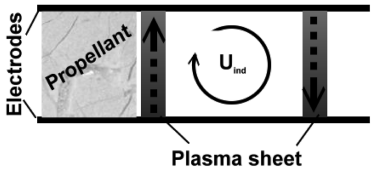

Fig. 10 Schematic of the induced voltage causing the formation of the second plasma sheet at the time the current passes zero.

is explained in Fig. 10 and occurs due to the strongly declining magnetic field and the resulting induced voltage, opposing this decline. Because the zero crossing is delayed when the probe is positioned within the resulting current loop, this phenomenon could be verified herein. The closer the probe is to the propellant surface, the higher the fraction of the second current sheet contributing to the registered magnetic field. The curve enveloping all measurements represents the maximum magnetic field registered, summing up contributions from both plasma sheets. In the further development of the graph, the phenomena discussed are repeated.

When comparing data from the SIMP-LEX breech-fed configuration to the APPT data presented by Koizumi et al. [5], magnetic field signals show very good accordance. A bank energy of 7.4 J creates a maximum of 0.24 T compared with 0.7 T at 80 J for SIMP-LEX. Qualitatively, the signals look very similar, implying that the presence of the probe between the electrodes has a minor effect on the magnetic field. Palumbo and Begun [6] found a maximum of 1.65 T at 81.9 J. They stated the presence of an induced current sheet, which could be confirmed in this study.

B. Comparison Between Side-Fed and Breech-Fed Configurations

Comparing the magnetic field signal from the side-fed and breech-fed configurations in Figs. 8b and 11b shows that the total discharge time increases from 20 to 45 μs. Further, the magnetic field in Fig. 11b does not level out; instead, it seems like a low-frequency signal is superimposed. This is probably due to additional electromagnetic coupling within the experimental setup. The probe signal under variation of the capacitor voltage can be seen in Fig. 11 along with the magnetic field signal derived. The magnetic field probe was situated at the propellant's exit plane, as shown in Fig. 7a. Five half-periods are discernible, compared to four measured with the breech-fed configuration. The variation of voltage yields the same effects: a higher capacitor voltage and bank energy is accompanied by an increase in magnetic field strength. Figure 12 shows the magnetic field distribution along the electrode axis, both outside and between the propellant bars. Outside the propellant bars, the signal starts at the propellant exit plane at 0 mm. At this point, the first plasma sheet has already formed and causes a peak before the first zero crossing in Fig. 11a indicates the sheet center reaching the probe. The first amplitude decreases as the probe is moved away from the propellant exit plane. As seen for the breech-fed signals, the side-fed signals converge to a joint envelope shortly before crossing the abscissa, though the envelope is not as distinct. Figure 12b investigates the behavior of the plasma sheet between the propellant bars. The maximum amplitude of −0.7 T recorded with the breech-fed configuration is matched at −22 mm, again corresponding with the probe position closest to the propellant. The magnetic field from the complete plasma current is registered at this position, because the current is downstream of the probe. A distinct first amplitude can be

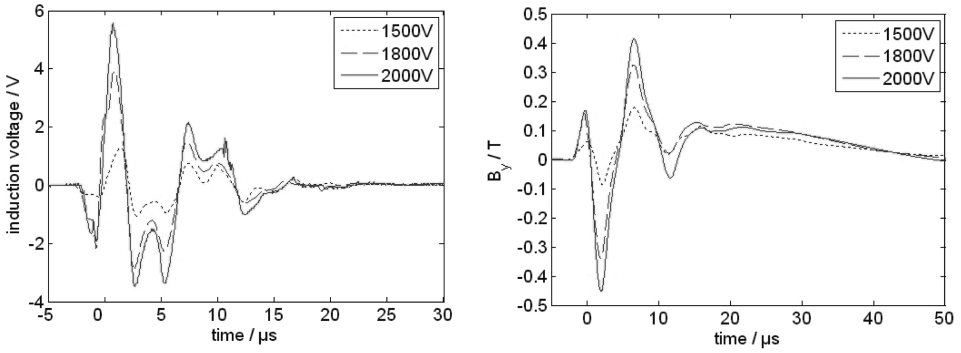

a) Signal from induction probe at different capacitor voltages **b) Corresponding magnetic field over time**

Fig. 11 Induction probe signal and magnetic field for different capacitor voltages, side-fed thruster configuration.

discerned at the position -9 mm, because a plasma sheet has already formed.

C. Investigation of the Propellant's Exit Plane

This section regards the magnetic field at four positions in the propellant exit plane perpendicular to the thruster's electrode axis, as seen in 7a. Between the V-shaped PTFE bars, the effective electrode width for the current is limited by the bars. After the current sheet passes the propellant exit plane, the entire electrode width is available to the current.

The overall peak of the magnetic field signal is recorded at the cathode ($y = 0, z = 5.5$), closely followed by the position in the middle between the electrodes. The peak of the magnetic field for the $y = 0$ mm position is lowest close to the anode ($y = 0, z = -5.5$). As seen in Fig. 13a, the probe signal at the edge of the electrode ($y = -20, z = 0$) lacks the first peak. This can be explained by the fact that, even though the discharge process starts about 2 μs earlier, the plasma sheet is only forming at this point.

The first zero crossing of signals, corresponding to different measurement points along the z axis, deviate slightly from each other. In particular, the plasma sheet seems to move across the probe close to the cathode about 0.75 μs earlier than across the one at the anode. The sheet canting suggested by this pattern agrees with what is observed in camera measurements. The plasma at the cathode is ahead of the one at the anode, as seen in Fig. 14. However, the difference of 0.75 μs seems too small when regarding the noticeable canting angle in Fig. 14 at plasma-sheet velocities on the order of $\sim$10 km/s. Current sheet canting has been studied by other authors [5,6,11]. In general, a magnetic field probe seems a suitable option to study this process further.

Figure 14 shows the magnitude of the magnetic field over time as three shaded bars for the upper, middle, and lower z position of the probe. These positions correspond to the cathode, electrode axis, and

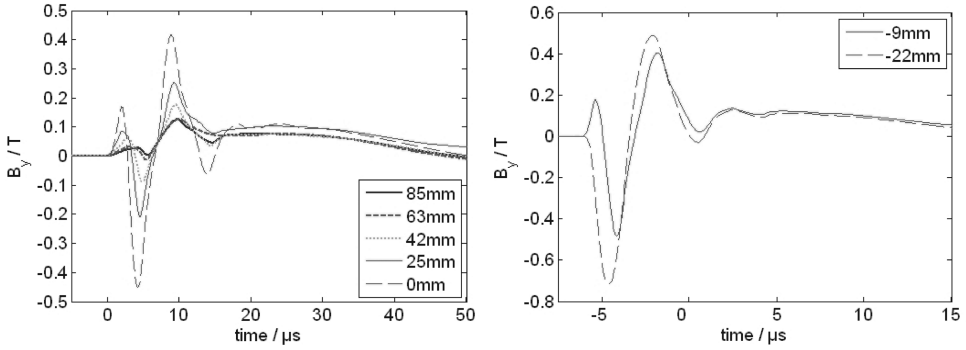

a) Magnetic field at points on the electrode axis **b) Magnetic field between the PTFE bars**

Fig. 12 Magnetic field along the electrode axis, outside and between the propellant bars, 2000 V bank voltage.

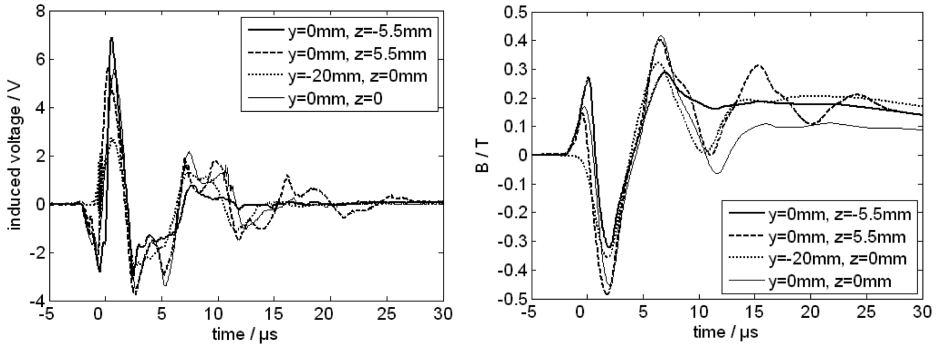

a) Induction probe signal **b) Magnetic field**

Fig. 13 Induction signal and magnetic field at propellant exit plane, positions indicated in Fig. 7a, 2000 V bank voltage.

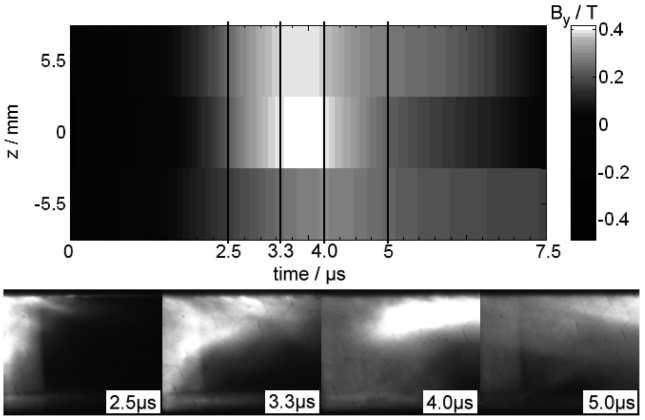

Fig. 14 Magnetic field intensity across electrode distance (top) and corresponding high-speed camera image (bottom).

the anode, respectively. All three measurement positions are on the line forming the intersection between the thrusters x–z-symmetry plane and the PTFE exit plane. The gray scales indicate the magnetic field intensity for all three probe positions over time. The four camera pictures on the bottom show a side view of the discharge channel at the times specified by the four vertical lines. In the pictures, the plasma flows from left to right, with the propellant to the left of the picture. The pictures were taken with a high-speed camera using an exposure time of 50 ns and a wavelength range of 380–900 nm. On the first picture, at 2.5 μs, the initial plasma has just passed the PTFE exit plane and can be seen as a straight glowing region reaching the two electrodes. Note that the center of the glowing area in the pictures must not necessarily correspond to the center of the accelerating plasma sheet. The second and third picture show the plasma propagation along the discharge channel. The glowing area is more pronounced at the upper cathode than the lower anode. This effect is mirrored in the magnetic field data displayed. A connection between strong magnetic forces and glowing areas was assumed. On the last picture, the plasma sheet has moved on, leaving a smaller, more even magnetic field at the propellant exit plane. The observation of faster plasma propagation near one of the electrodes is associated with the effect of plasma-sheet canting as mentioned previously.

D. Comparison of Modeled and Measured Magnetic Field

The model used for the magnetic field extended the slug model by a numeric 3-D grid calculation and the law of Biot–Savart as discussed previously. The model of the magnetic field was evaluated against the measurements. Because the slug model assumes a plasma sheet of even shape, constant thickness, and no canting, the thruster's breech-fed configuration was chosen for evaluation. The magnetic field was obtained at two positions on the electrode axis. The simulation of the magnetic field between the electrodes depends on both the plasma position and the discharge current as functions of time. This information was simulated by means of the slug model. Comparison of the calculated and measured magnetic field, 5 and 27 mm away from the PTFE surface, can be seen in Fig. 15.

The curves in Fig. 15a show good correlation in wavelength up to about 10 μs, though the amplitudes of the model are lower by a factor of about 2. After 15 μs, the model does not agree with the recorded signal anymore. Whereas the model follows a damped sinusoidal curve, the measured magnetic field is zero. The strong damping is probably due to a rise in the discharge circuit's ohmic resistance; an effect unaccounted for in the model. At about 5 and 10 μs, the model's magnetic field is disrupted. This occurs when the model switches to the calculation of the next plasma sheet and the plasma velocity and position is set to zero. The probe is always inside the modeled circuit; the magnetic field is only zero when the current is zero. As confirmed from current measurements, this indicates the current frequency is modeled correctly. However, simulation in Fig. 15b does not agree with the measurement. The first half-cycle is predicted to be too long. The zero crossings are not correlated with the recorded signal. Further, the disruptions are far more obvious. Because the current was shown to agree well with the measurements, the plasma position accounts for the poor result. Apart from the current, the plasma position is influenced by the massbit and the circuit's inductance. Whereas the inductance was significantly ameliorated within the slug model, the massbit distribution remains unknown. In addition, the contributions from the electrodes are to be extended to the volume ahead of the plasma sheet for improving the accuracy of the model. Finally, the crude assumptions made in the slug model contribute to the lack of agreement between the model and the measurement. Better results are expected in the future by evaluating the model's plasma position. This is to be achieved by high-speed camera pictures and intrusive current density probes.

VI. Conclusions

To understand the plasma discharge and acceleration process within a PPT better, a two-way approach was used. On the model side, the temporal development of the thruster's magnetic field and the resulting inductance were investigated. The magnetic field was calculated between the electrodes using the law of Biot–Savart. For this calculation, contributions of the entire discharge circuit were considered, in particular, the electrodes and a plasma sheet of 3 mm thickness. The discharge current was calculated using the slug model. Model predictions of the magnetic field at two positions of the thruster's breech-fed configuration were compared with experimental results. The magnetic field distribution for the probe position closest to the propellant surface showed good accordance. The angular frequency was mirrored well, even though the magnetic field predicted by the model was too low by a factor of 2. For the position further away from the propellant surface, the agreement was poorer. The distribution of the thruster's inductance is a temporal function of both the discharge current and magnetic field. Further work correlating the magnetic field with the discharge current promises more accurate modeling of the discharge process for optimization of

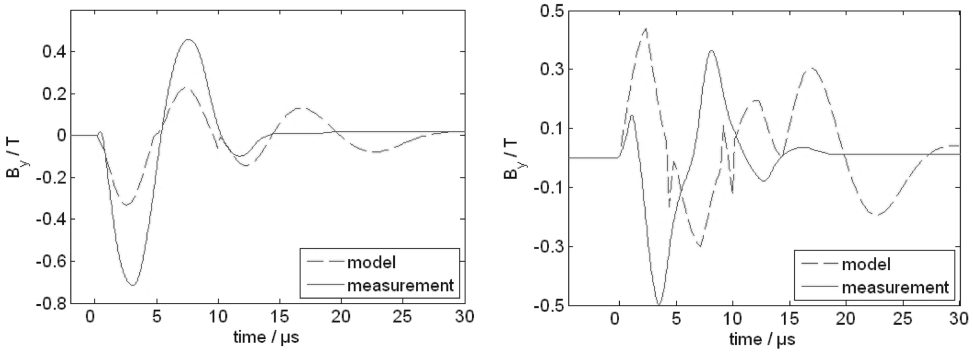

a) Magnetic field distribution 5 mm from the PTFE surface

b) Magnetic field distribution 22 mm from the PTFE surface

Fig. 15 Comparison of magnetic fields at two positions on the electrode axis of the thruster's breech-fed configuration, 2000 V.

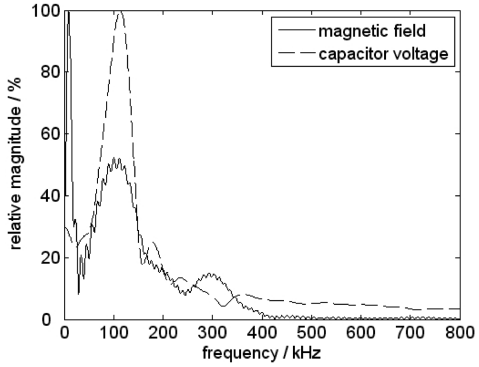

Fig. 16 Frequency spectrum of a magnetic field signal.

the thruster in the future. In addition, to improve the model, the function of the current over time must be modeled more precisely.

On the experimental side, the acceleration process was investigated using an improved method for determining magnetic field strengths in electromagnetic environments. A magnetic field induction probe was built. Successful calibration against a Helmholtz coil was achieved by comparing theoretically and experimentally induced voltage as a function of frequency. The frequency range of the probe was verified by comparing the Fourier spectrum of the magnetic field and discharge voltage signals. An exemplary spectrum is given in Fig. 16. Note that the magnitudes are normalized to the maximum magnitude. The calibration procedure improves accuracy of measuring magnetic fields by revealing the probe's induction response.

The experiments were carried out at positions on the electrode axis of both a side-fed and a breech-fed thruster configuration. In addition, the propellant exit plane of the side-fed configuration was investigated. The magnetic field data correlated well with camera pictures, recorded from earlier investigations with the same thruster geometry.

It was not possible to derive a current sheet velocity for the side-fed configuration from the magnetic field zero crossings because of low-frequency interferences. However, breech-fed configuration signals were free from interference, and a velocity of 20 km/s could be deduced for the first current sheet. Further, comparison between the zero crossing of the magnetic field close to the cathode and anode suggested that current sheet canting can be detected from magnetic field studies. This phenomenon will be addressed in a systematic approach in future studies.

From the variation of the probe position along the electrode axis, it is possible to conclude that an electric field is induced, confirming the findings of Palumbo and Begun [6]. This causes the second plasma sheet to start forming before the discharge current changes direction.

Acknowledgments

We gratefully acknowledge the funding of the German Aerospace Center Deutsches Zentrum für Luft- und Raumfahrt under contract number FKZ-50-JR-0446. We further thank Manfred Hartling who was a great asset concerning the electric setup.

References

[1] Lunar Mission BW1 Project Team, "The Stuttgart Moon Orbiter Lunar Mission BW1," *First CEAS European Air and Space Conference Century Perspectives*, Deutsche Gesellschaft für Luft- und Raumfarht, Bonn, Germany, 2007.

[2] Burton, R. L., and Turchi, P. J., "Pulsed Plasma Thruster," *Journal of Propulsion and Power*, Vol. 14, No. 5, 1998, pp. 716–735. doi:10.2514/2.5334

[3] Scharlemann, C., "Investigation of Thrust Mechanisms in a Water Fed Pulsed Plasma Thruster," Ph.D Thesis, The Ohio State Univ., Columbus, OH, 2003.

[4] Dawbarn, R., McGuire, R. L., Steely, S. L., and Pipes, J. G., "Operating Characteristics of an Ablative Pulsed Plasma Engine," Arnold Engineering Development Center AEDC-TR-82-9, AFRPL-TR-82-17, July 1982.

[5] Koizumi, K., Ryosuke, N., Komurasaki, K., and Arakawa, Y., "Plasma Acceleration Process in an Ablative Pulsed Plasma Thrusters," *Physics of Plasmas*, Vol. 14, No. 3, 2007, p. 033506. doi:10.1063/1.2710454

[6] Palumbo, D. J., and Begun, M., "Plasma Acceleration in Pulsed Ablative Arc Discharges," Final Rept. Period 1974–1977, Fairchild Industries, New York, 1977.

[7] Jahn, R. G., *Physics of Electric Propulsion*, Series in Missile and Space Technology, McGraw–Hill, New York, 1968.

[8] Feynman, R. P., Leighton, R. B., and Sands, M. L., *Lectures on Physics*, Vol. 2, Addison–Wesley, Reading, MA, 1989.

[9] Philipps, R. C., and Turner, E. B., "Construction and Calibration Techniques of High Frequency Magnetic Probes," *Review of Scientific Instruments*, Vol. 36, No. 12, 1965, p. 1822. doi:10.1063/1.1719473

[10] Demtröder, W., *Experimentalphysik 2, Elektrizität und Optik*, Springer–Verlag, Berlin, 2004, Band 2, 3, ISBN 3-540-20210-2.

[11] Markusic, T. E., and Choueiri, E. Y., "Phenomenological Model of Current Sheet Canting in Pulsed Electromagnetic Accelerators," *28th International Electric Propulsion Conference*, Paper 2003-0293, Electric Propulsion and Plasma Dynamics Lab., Princeton, NJ, 2003.

A. Tumin
Associate Editor